CHAPTER 4

APPLICATION OF PURE ZnO AND WO_3-DOPED ZnO FOR USE AS GAS SENSORS

4.1 Introduction

Chemical sensors with metal oxides as sensing material have been around for a long time as a low cost alternative for gas detection devices. However, they have, to some extent, suffered from limitations in sensitivity, selectivity and stability when compared to more expensive alternatives. Recent advances in nanotechnology and nanomaterials have fostered fabrication techniques that can be harnessed to increase the response and performance of these materials. This is because their performance is governed by the exposed surface area; the gas sensing mechanism being due to reactions that occur at the sensor surface. Better adsorption-desorption phenomena on higher surface area would enhance the sensitivity of gas sensor. Therefore, gas sensor based on nanostructured materials should be able to detect sensing gas molecules at lower concentration and present better sensing properties than gas sensors based on bulk materials [1-2].

ZnO and WO_3 are well-known transition metal-oxide materials which have promising gas-sensing performance, primarily due to their catalytic properties. The combination of these metal oxides with an appropriate proportion is a useful approach to enhance gas-sensing performance. Promising results have been reported from recent studies on WO_3/ZnO films prepared by the sol-gel method [3]. Preparation technique can considerably affect the physical, chemical, and gas sensing properties of the mixed oxide sensor because these peculiarities rely on the essential surface activity of the layers. One of interesting preparation techniques is Flame Spray

Pyrolysis (FSP) [4-7] which is a cost-effective and versatile process for controlling the production of nanoparticle materials. This process has been demonstrated as one-step, suitable for dry synthesis of high surface area, and highly efficient for noble metal laden catalysts. Furthermore, the specific surface area increased with increasing oxidant flow rate leading to a reduction in spray flame length, which resulted in shorter residence time and allowed less time for particle growth [4]. These advantages of flame aerosol synthesis prompted us to apply FSP for production of pure ZnO and WO_3-doped ZnO nanoparticles for use as gas sensors.

The aim of the present work is to investigate the performance of gas sensor based on pure ZnO and WO_3-doped ZnO nanoparticles synthesized by FSP on NO_2, C_2H_5OH, CO and H_2 which are dangerous and poisonous gases.

4.1.1 Operation principle of the semiconducting gas sensors [8-10]

The principle subject to which these sensors operate can be summarized as follows. There is a finite density of electron donors (e.g., adsorbed hydrogen) and/or electron acceptor (e.g., adsorbed oxygen) bound to the surface of a wide-bandgap semiconducting oxide, such as SnO_2 or ZnO. They represent surface states which can exchange electrons with the interior of the semiconductor, thus forming a space-charge layer situated close to the surface as in Figure 4.1. The position of the surface state relative to the Fermi level of the semiconductor depends on its affinity to electrons. If its affinity is low, it will lie below the Fermi level and donate electrons (reducing agent) to the space-charge region. If it is an acceptor, it will be positioned above the Fermi level and extract electrons (oxidizing agent) from the space-charge region. By changing the surface concentration of the donors/acceptors the conductivity of the space-charge region is modulated.

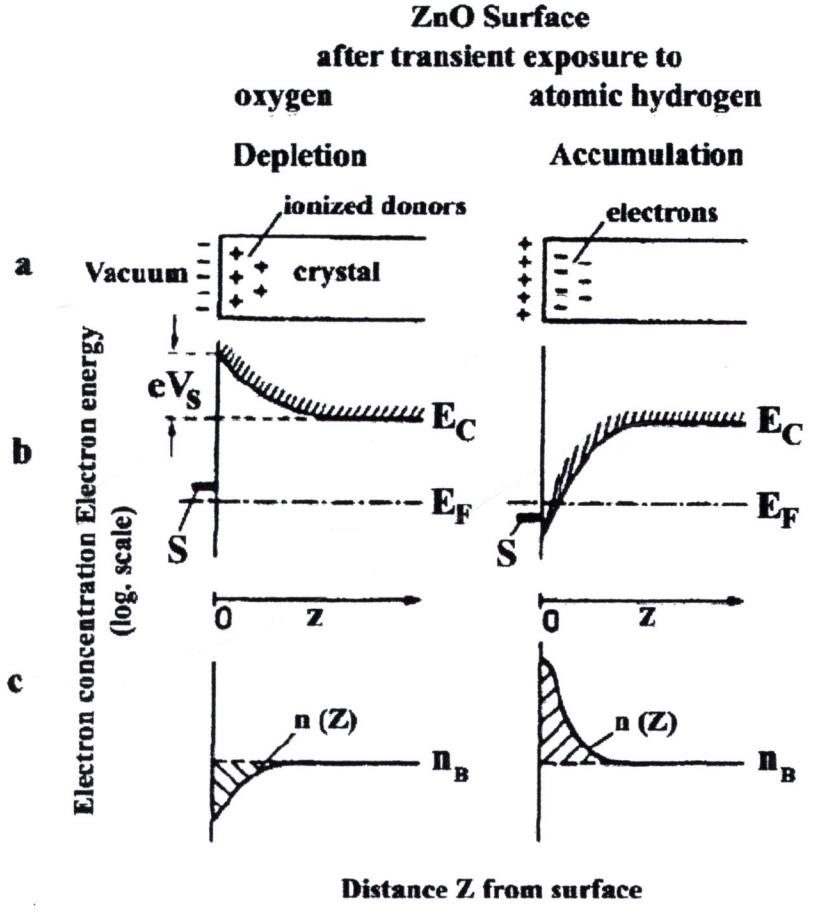

Figure 4.1 Space-charge modulations by adsorption in a semiconducting n-type semiconductor oxide sensor [10]

In an n-type semiconductor, such as SnO_2 and ZnO, the majority carriers are electrons therefore the change in surface conductivity $\Delta\sigma_s$ is given from Equation 4.1 in the form:

$$\Delta\sigma_S = e\mu_s\Delta n_s \tag{4.1}$$

where e is the electron charge and μ_s is the electron mobility at the surface. The excess density (Δn_s) of charge carriers in the space-charge region of thickness d is obtained by integrating the difference between the electron density in the space-charge region and in the bulk (n_b) over the thickness d:

$$\Delta n_s = \int_0^d [n(z) - n_b]dz \tag{4.2}$$

The change in surface conductance ΔG_s is then:

$$\Delta G_s = \Delta\sigma_s W/L \tag{4.3}$$

For an *n*-type semiconductor (such as ZnO) an increase in the surface concentration of the electron donor (e.g. hydrogen) will therefore increase the conductivity. On the other hand, adsorption of hydrogen on a *p*-type oxide (such as CoO) will decrease its conductivity by the same argument.

The bulk conductance which is not modulated by the surface reactions is represented by a parallel conductor (Figure 4.2):

$$G_b = nbe\mu_b Wd/L \tag{4.4}$$

The terms in Equation 4.4 have the same meaning as those in Equation 4.2 and 4.3. Subscript *b* refers to the bulk quantities while *d* is the total thickness of the oxide layer. Since the overall conductance is measured, it is advantageous to have the films as thin as possible.

The relative change in the conductance of the whole device is obtained from Equation 4.2, 4.3 and 4.4 and by assuming that $\mu_b \sim \mu_s$. Hence:

$$\Delta G / G = \Delta n_s / n_b d \tag{4.5}$$

For the value of the relative conductance change (high sensitivity), it is necessary to have a low density of bulk carrier and a thin film. The space-charge thickness is typically 100-1000 Å, depending on the doping. As an example let us consider a typical value of the excess surface-state density $n_s = 10^{12}$ electrons cm^{-2} and the bulk density $n_b = 10^{17}$ electron cm^{-3}. This means that for a 100 μm thick film the sensitivity $\Delta G_s/G_b = 10^{-3}$. However, for d = 100 Å, the sensitivity is 10 and for

thin films (< 1000 Å) the space-charge region extends throughout the whole film thickness.

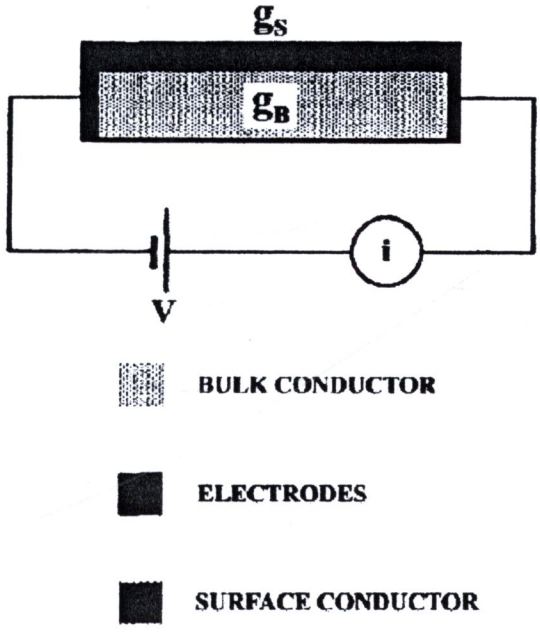

Figure 4.2 Schematic representation of a semiconducting oxide sensor with bulk (g_B) and surface (g_S) conductivities shown [10].

The most widely accepted explanation for surface conductivity change of semiconducting oxide is that negatively charged oxygen adsorbates play an important role in detecting gases such as H_2 and CO. Actually, several kinds of oxygen adsorbates, such as O_2^-, O^- and O^{2-}, are known to cover the surface of semiconducting oxides in air. Yamazoe et al. [11] reported that oxygen showed the formation of four kinds of oxygen species on SnO_2 surfaces which desorb around 80°C (O_2), 150 °C (O_2^-), 560°C (O^- or O^{2-}) and above 600 °C (a part of lattice oxygen) respectively. Of these, O^- is the most reactive with reducing gases in the temperature range of 300-500 °C, in which most semiconductor gas sensors are operated. The variation in surface coverage of O^- therefore is believed to dominate the sensor response. In the case of n-

type semiconducting oxides, the formation of this oxygen adsorbate builds space charge regions on the surfaces of the oxide grains, resulting in an electron-depleted surface layer due to the oxygen adsorbates as follows:

$$O_2(g) + 2e^- = 2O^-(s) \tag{4.6}$$

The resistance of an n-type semiconducting oxide gas sensor in air is therefore high, due to the development of a potential barrier. The space charge layer (W) can be defined using Poisson's equation as follows:

$$W = \frac{Q_S}{e \cdot N_D} = [\frac{2 \cdot K\varepsilon_0 \cdot \Delta\phi_S}{e \cdot N_D}]^{1/2} \tag{4.7}$$

Here, Q_S and N_D are surface charge and the number of ionized donor states per unit volume, and K, ε_0, and $\Delta\phi_S$ denote the static dielectric constant of the oxide, the permittivity of the vacuum, and the surface potential barrier height. With typical values ($K\varepsilon_0 \sim 10^{-12}$ F/cm, $N_D \sim 10^{18} - 10^{20}$ cm^{-3} and $\Delta\phi_S \sim 1$V), the space charge layer thickness is generally around 1 – 100 nm.

Figure 4.3(a) shows a schematic of a few grains of porous semiconducting oxide and the space charge region around the surface of each grain and at inter-grain contacts. The space charge region, being depleted of electrons, is more resistive than the bulk. The band model of Figure 4.3(b) shows potential barriers formed at inter-grain contacts.

When the sensor is exposed to an atmosphere containing reducing gases at elevated temperatures, the oxygen adsorbates are removed by the reduction reaction, so that the steady-state surface coverage of the adsorbates is lowered. For example, if the sensor is exposed to H_2 atmosphere, the reaction will be as follows:

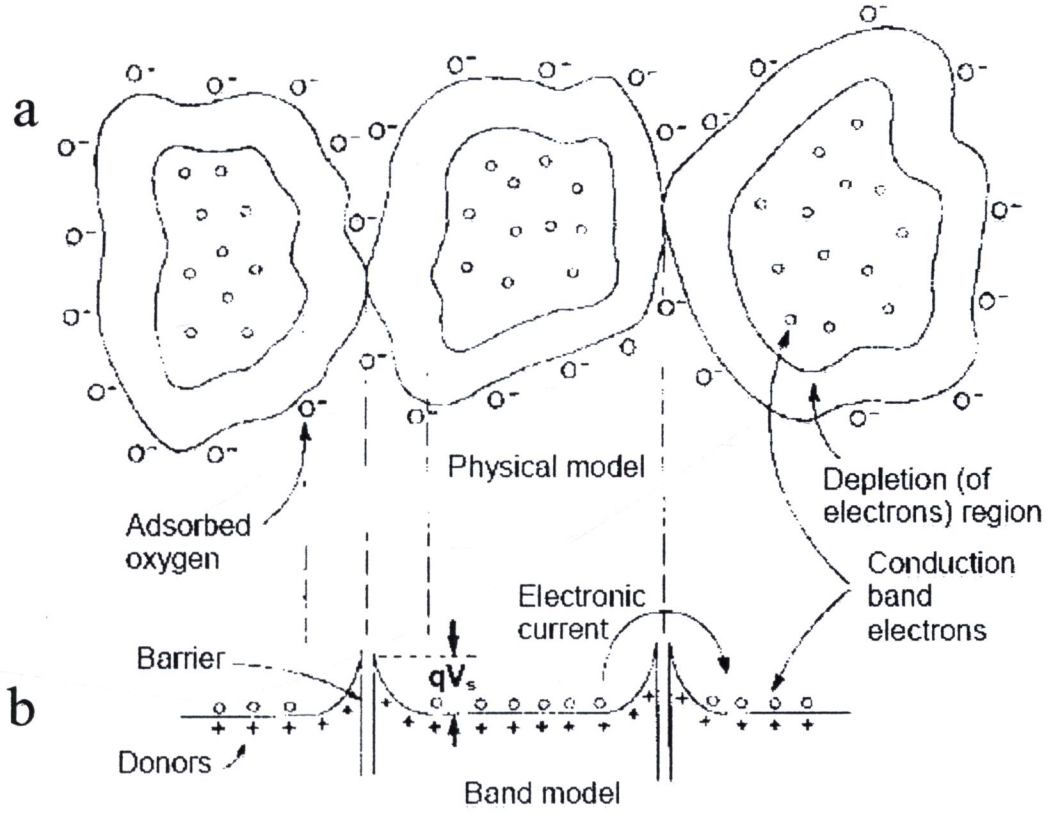

Figure 4.3 Grains of semiconductor, to show how the inter-grain contact resistance appears. [12]

$$O^{-}(s) + H_2 \rightarrow H_2O + e^{-} \tag{4.8}$$

During this process, the electrons trapped by the oxygen adsorbates return to the oxide grains, leading to a decrease in the potential barrier height and drop in resistance. Figure 4.4 shows the change of the potential barrier in air and reducing gas environments due to the variation of the space charge region at each grain boundary, contact and surface of semiconducting oxide. These resistance changes exposed to reducing gases are used as the measurement parameter of the semiconductor gas sensor [12].

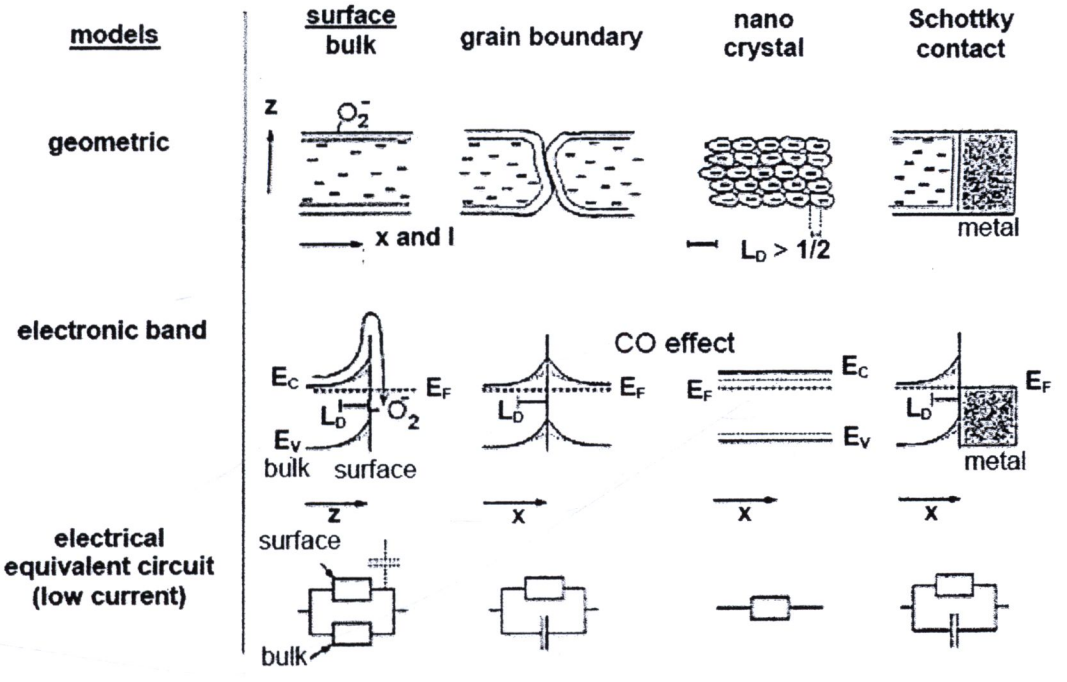

Figure 4.4 Influence of particle size and contacts on resistances and capacitances in thin films are shown schematically for a current flow I from left to right [12].

One of the most important factors affecting sensing properties is the actual grain or crystallite size D of the sensor materials in conjunction with the space charge depth L. Three kinds of resistance-control models have been proposed, which assume that a sensor consists of a chain of uniform crystallites of size D connected mostly with each other through necks and sometimes by grain boundaries, as shown in Figure 4.5. When D is less than 2L, the grain resistance dominates the resistance of the whole chain and in turn, the sensor resistance, so that grains themselves (grain control) control the sensitivity. Among the three models, grain control is the most sensitive condition. Thus, smaller grain sizes would be more sensitive than larger ones [13].

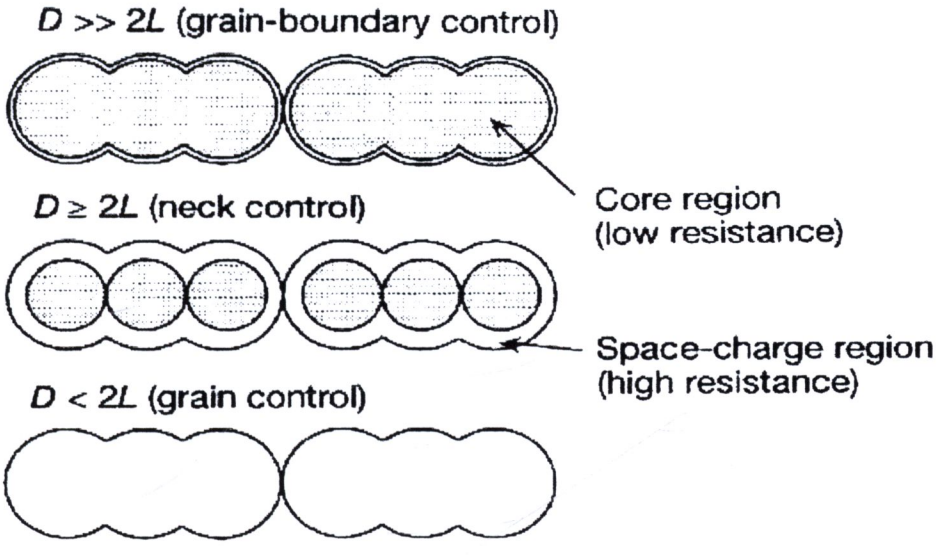

Figure 4.5 Schematic models for grain-size effects [13]

For most conventional semiconducting oxide materials, the particle size is considerably greater than the depth of the space charge, and electrical conduction is controlled by the grain boundaries. However, nanocrystalline materials can be produced which offer greatly reduced grain size, so that the depletion layer has similar dimensions to the particle radius. Under these conditions, oxygen adsorption will result in grains fully depleted of conduction-band electrons. Therefore, these materials can be potentially used to produce highly sensitive gas sensors

Since the charge carriers in p-type semiconducting oxides are positive holes, the resistance in air is low because of the formation of negatively charged oxygen adsorbates, and the extraction of electrons from the bulk eventually enhances the concentration of holes in the grain surface. Then, the consumption of oxygen adsorbates by reaction with reducing gases leads to an increase in resistance, which is the reverse of the case for n-type semiconducting oxides. Conversely, the adsorption of oxidizing gases on p-type semiconducting oxides results in a decrease in resistance.

4.1.2 Sensor requirements and characteristics [8, 10, 14]

The semiconductor sensing properties rely on reactions between semiconductor and gases in the atmosphere that can make a change in the semiconductor resistance. The adsorption reaction of gases at surface leads to a change in the conductivity. Firstly, oxygen in the atmosphere adsorbs and extracts electrons from the conduction band of the semiconductor. When the desired concentration of gases is introduced, many possible processes can occur. The gases may react with the oxygen adsorbed on the surface or with the semiconductor surface, or with both; for an n-type semiconductor the resistivity increases due to electron capture by an oxidizing gas and decreases with the presence of a reducing gas owing to electron transfer into the conduction band, while the opposite holds for a p-type semiconductor. The key characteristics of gas sensor performance are selectivity, sensitivity and response time.

4.1.2.1 Selectivity

The selectivity can be defined as the ability of a sensor to respond primarily to only on species in the presence of other species. This is the most important characteristic of sensors; the ability to discriminate between different substances. Such behavior is principally a function of the selective component, although sometimes the operation of the transducer contributes to the selectivity. This factor is the essence of sensors. It is the rate to find a sensor which will respond to only one analysis, although some do exist. It is more usual to find a sensor that will respond mainly to one analysis, with a limited response to other similar analysis. Alternately, the response may be to a group of analysis of similar chemical structure, such as carbonyl compounds.

4.1.2.2 Sensitivity

The gas sensing sensitivity of n-type semiconductor based conductometric gas sensor to reducing gases (e.g. C_2H_5OH, NH_3, SO_2, CO and propanol) are normally defined as the ratio, $\Delta R/Rg$, of the resistance change (ΔR) due to gas introduction to the resistance when the gas is present (Rg) while the response to oxidizing gases (e.g. NO_2) are defined as the ratio, $\Delta R/R_0$, of the resistance change to the resistance in air (R_0). The sensitivity of n-type semiconductor gas sensor for reducing gases and oxidizing gases are shown in equations 4.9 and 4.10, respectively. For p-type semiconductor gas sensor, the definitions are reversed. The gas-sensing sensitivity was calculated from dynamic variation of the conductance due to gas pulses introduction and plotted versus various parameters including temperature and gas concentration.

$$S = \frac{\Delta R}{R_g} = \frac{R_0 - R_g}{R_g} \tag{4.9}$$

$$S = \frac{\Delta R}{R_0} = \frac{R_g - R_0}{R_0} \tag{4.10}$$

4.1.2.3 Response and recovery time

Many analytical devices require some "settling-down" time, i.e. time to allow the system to come to equilibrium, the response time. This is true to some extent with many chemical methods. However, with sensors of a chemical or biochemical nature this response time is greatly offset by the simplicity of the measurement and the minimal sample preparation time. Normally, the response times can vary from a few seconds to a few minutes. Up to 5 min may be acceptable, but if the time exceeds 10 min this may be too long. Normally, the response time, T_{res} is defined as the time required until 90 % of the response signal is reached

Very much related to the response time is the recovery time. The recovery time is the time that elapses before a sensor is ready to be used for another sample measurement. The resulting response time may be immediate or it may be that after one measurement the sensor system has to rest the resume its base equilibrium before it can be used with the next sample. In many publications, these times are combined and the result is given as the number of samples that can be analyzed per hour, which obviously is the main practical point at the end. In this research, the response and recovery times are important parameters for designing sensors for the desired application. The response/recovery times are defined as the time required for adsorption and desorption of oxygen on, or from the sensor surface to reach the saturation or to reduce the conductivity back to the baseline conductance. A good sensor is the one that shows a short response and recovery time. Normally, the recovery times, T_{rec} denotes the time needed until 90 % of the original baseline signal is recovered. The response and recovery time of n-type semiconductor for reducing gas can be calculated (Equation 4.11 and 4.12) as follows:

$$T_{res} = [T_{R_0} - \{(T_{R_0} - T_{R_g})\} \times \frac{90}{100}] - T_{R_0} \qquad (4.11)$$

$$T_{rec} = [T_{R_g} + \{(T_{R_0} - T_{R_g})\} \times \frac{90}{100}] - T_{R_g} \qquad (4.12)$$

4.1.3 Literature review

ZnO gas sensing properties have been investigated by many researchers.

In 2001, Nunes et al. [15] made ZnO thin films by spray pyrolysis for methane gas sensing. It was found that ZnO films showed good detection performances for methane and these films can work at 373 K. In 2004, Cheng et al. [16] prepared ZnO thin films by sol-gel dip coating method. The gas-sensing properties of the ZnO films for alcohols with different chain lengths were measured at room temperature. The thin films exhibited high sensitivity and rapid response–recovery characteristics to methanol, ethanol and propyl alcohol. The film could detect methanol, ethanol and propyl alcohol vapor as low concentration as 1, 10, and 0.5 ppm, respectively.

The effect of film thickness on sensor performance was investigated by Chang et al. [17]. They fabricated ZnO films using rf reactive sputtering on a SiO_2/Si wafer with variable thickness (65 nm to 390 nm). The best sensitivity and fastest response were obtained with the thinnest film (65 nm).

The gas responses of chemically deposited ZnO films were investigated by Mitra et al. [18]. A high sensitivity was observed for 3 vol.%. H_2 at the temperature of 150 °C. However, the sensor exhibited very poor recovery characteristics due the surface reduction of ZnO. The ZnO sensor showed higher sensitivity to liquid petroleum gas (LPG) in the 0.4-1.6 vol.% concentration in air. Moreover, sensing behaviors of ZnO thin films to ethanol prepared by spray pyrolysis was reported by Sahay et al. [19]. The sprayed ZnO thin films showed considerable changes in their resistances when exposed to ethanol with different temperature. It was found that the film layers of 20 μm in thickness showed sensitivity in terms of rather high ethanol concentration (1000-5000 ppm) at 150-350°C. It was observed that the sensitivity increased with increasing operating temperature. At higher ethanol concentration, the

sensitivity increased rapidly with increasing operating temperature. Response and recovery times were found to be sensitively dependent upon the operating temperature.

In order to enhance the gas sensing properties of the sensors, many of metal ions were examined as dopants in ZnO gas sensor. For instance, in 1999, the ZnO thick film sensor was investigated by Rao et al [20]. They prepared the calcined powders of undoped and doped ZnO with Pd, Fe and Ru for thick film NH_3 sensors. The Pd-ZnO exhibited good sensitivity and response time to NH_3 at room temperature. In 2001, ZnO thin film sensors doped with Al, In, Cu, Fe, and Sn using spray pyrolysis technique were prepared by Paraguay et al. [21]. It was found that these films showed good sensitivity to ethanol vapor (as high as 190). Sn and Al dopants gave the highest sensitivity in the working temperature of 675 K. Moreover, in 2005, Pd-doped ZnO nanotetrapods using thermal evaporation method for ammonia sensors were prepared by Wang et al. [22]. It was found that Pd-doped ZnO nanotetrapods showed high sensitivity to ammonia in the range of 30–1000 ppm. The response time of the sensor was as fast as $\approx$ 2 s at any concentration (40–1000 ppm) of ammonia gas.

In 1999, the thick film sensor of WO_3 for NO_2 gas detection was reported by Chung et al. [23].The degree of oxygen deficiency in the WO_3 sensor also affected sensor properties and the optimum oxygen content of WO_3 which was necessary to get high sensitivity for NO_2. The WO_3 thick film fired at 700°C and operated at 100°C showed excellent sensor properties

In 2008, various compositions of gas sensing films using the combinatorial deposition of SnO_2, ZnO, and WO_3 sol solutions were prepared by Kim et al. [24]. The results showed that the sensor composition could be conveniently optimized for

the selective gas detection by the combinatorial deposition of SnO_2, ZnO and WO_3 oxide sols. From the gas responses to C_2H_5OH, CH_3COCH_3, CO, C_3H_8, H_2, and NO_2, it was found that the selective detection of C_2H_5OH could be attained in the SnO_2–ZnO composite sensor at 300 °C and ZnO–WO_3 composite sensor at 400 °C.

Silica nanoparticles at high production rates up to 1.1 kg/h were synthesized by Müller *et al.* [25]. The production of ZnO prepared by FSP method using zinc acrylate as a starting material dissolved in methanol and acetic acid mixtures (94:6 vol%) was reported by Tani *et al.* [26]. The results showed that the average primary particle diameter was in the range of 10 to 20 nm. Moreover, high specific surface area Ag-doped ZnO photocatalysts synthesized by FSP were reported by Height *et al.* [27]. The photocatalyst powders consisted of monocrystalline zinc oxide primary particles of 8–25 nm supporting nanocrystals of silver metal around 5–20 nm for Ag loadings of 1–5 at.%. Furthermore, ZnO nanoparticles synthesized by FSP (5/5) were reported by Height *et al.* [28]. The pure ZnO contained mainly spherical particles with diameters of 20 nm with occasional rod-like structures. These advantages of flame aerosol synthesis prompted us to apply FSP for production of pure ZnO and WO_3-doped ZnO nanoparticles and investigate the performance of gas sensors based on pure ZnO and WO_3-doped ZnO nanoparticles on NO_2, C_2H_5OH, CO and H_2.

4.2 Experimental

4.2.1 Chemical

Pure ZnO and WO_3-doped ZnO gas sensing films were prepared using chemicals as follows:

- Ethyl cellulose (Fluka, 30-60 mPa·s)
- Terpineol (Aldrich, 90%)

4.2.2 Apparatus

Pure ZnO and WO_3-doped ZnO gas sensing films were prepared and tested using the equipment as follows:

- Al_2O_3 substrates interdigitated with Au electrodes (Au/Al_2O_3; 5x 4 x 0.1 mm; National Electronics and Computer Technology Center, Thailand)
- Spin coater (Laurell, WS-400B-6NPP-LITE)
- Three-zone tube furnace (Lenton, PTF 15)
- Lab-set gas sensor measurement (National Electronics and Computer Technology Center, Thailand)
- Scanning electron microscope & EDS (JSM-6335F, JEOL)

4.2.3 Preparation of gas-sensing films

Gas-sensing films were prepared by mixing the nanoparticles into an organic paste composed of ethyl cellulose (Fluka, 30-60 mPa·s) and terpineol (Aldrich, 90%), which acted as a vehicle binder and solvent, respectively. The resulting paste was spin-coated on Al_2O_3 substrates with predeposited interdigitated Au electrodes. The films were then annealed at 400°C using three-zone tube furnace for 2 hours with

heating rate of 2 °C/min for binder removal. The ZnO thin films on Al_2O_3 substrates with interdigitated Au electrodes after annealing for 2 hours and cross sectional view of their structure are shown in Figure 4.6.

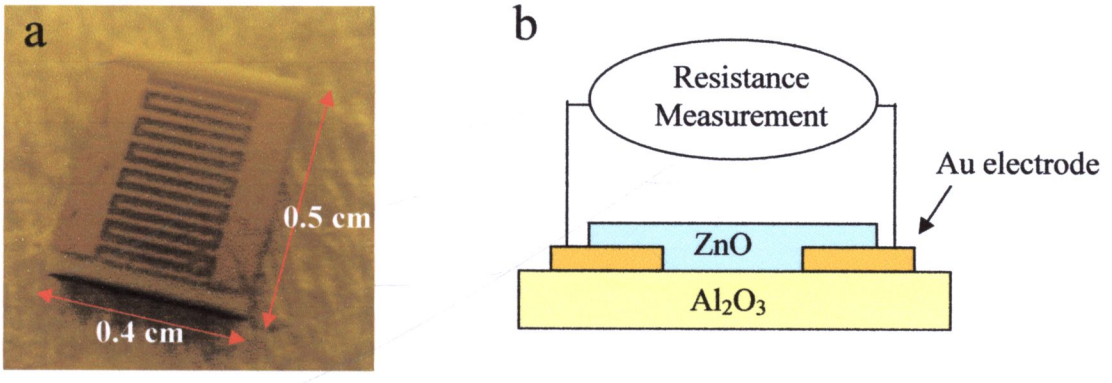

Figure 4.6 (a) ZnO thin film on Al_2O_3 substrates with interdigitated Au electrodes (b) Schematic cross-sectional view of ZnO gas-sensing film

4.2.4 Characterization of gas-sensing films

The gas-sensing characteristics of metal oxide nanoparticles were characterized towards NO_2, C_2H_5OH, CO and H_2. The flow through technique was used to test the gas-sensing properties of these sensors. A constant flux of synthetic air of 2 l/min was used as gas carrier into which the desired concentration of pollutants dispersed in synthetic air was mixed. All measurements were conducted in a temperature-stabilized sealed chamber at 20°C under controlled humidity. The external NiCr heater was heated by a regulated dc power supply to different operating temperatures. The operating temperature was varied from 300°C to 400°C. The resistances of various sensors were continuously monitored with a computer-controlled system by voltage-amperometric technique with 5 Volt dc bias (source-measure unit, keithley 2700) and current measurement through a picoammeter. The

sensor was exposed to a gas sample for 15 min for each gas concentration testing and then the air flux was restored for 25 min. The target gas concentration was varied from 1 to 50 ppm for NO_2, from 100 to 1,000 ppm for C_2H_5OH, from 50 to 1,000 ppm for CO and from 500 to 10,000 ppm for H_2. The experimental set up for gas testing was shown in Figure 4.7.

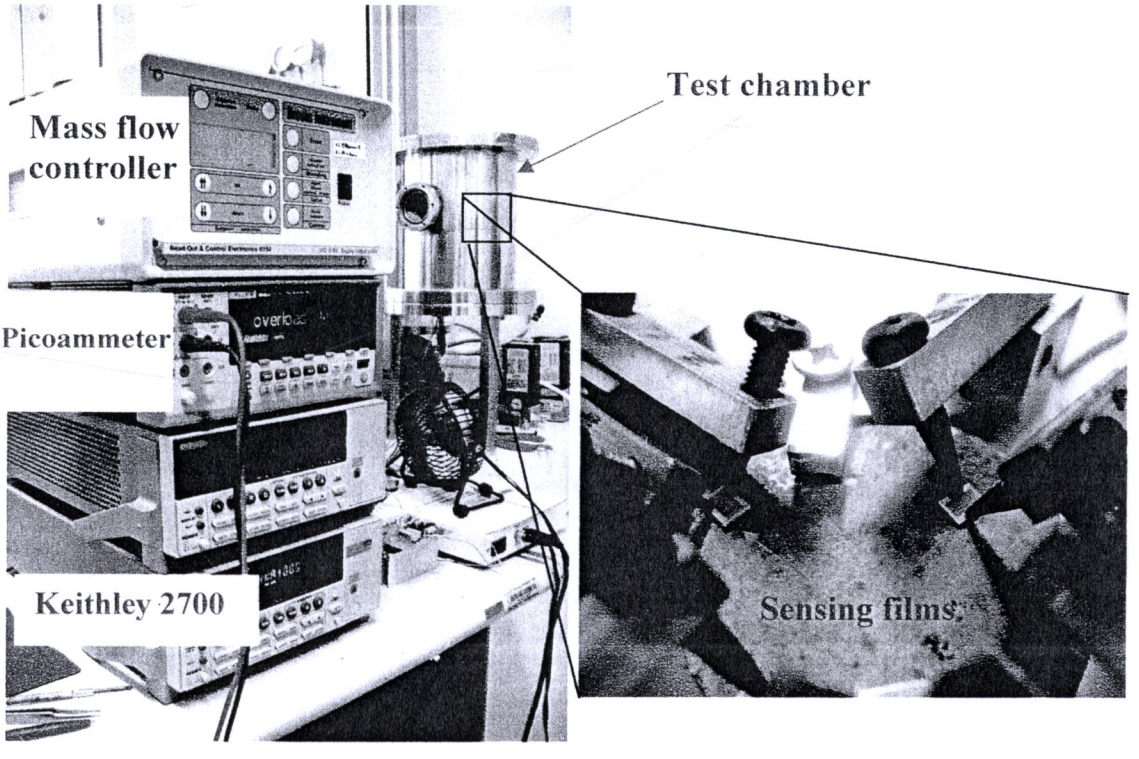

Figure 4.7 Gas sensor measurement setup

4.3 Results and discussion

4.3.1 X-ray diffraction analysis

The phase of gas sensing film based on flame-made 0.75 mol% WO_3-doped ZnO nanoparticles after anneal and sensing test at 400 °C were analyzed by X-ray diffraction spectroscopy (XRD, Philip X' Pert PRO PW 3719) using CuKα radiation at 2θ = 20-80° with a step size of 0.06° and a scanning speed of 0.72°/min as shown in Figure 4.8. It was found that this gas sensing film was highly crystalline, and its peaks can be confirmed to be the hexagonal structure of ZnO, which match well with the

JCPDS file No. 89-0510 [29]. The diffraction patterns of Al_2O_3 and Au from substrate were also visible in this sample, which match well with the JCPDS file No.82-1468 [30] and 04-0784 [31], respectively. Amorphous phase of ZnO and WO_3 peaks were not found in these patterns. It can be assumed that concentrations of WO_3 were too low and the sizes of WO_3 particles too small, which affected the WO_3 peaks appearance.

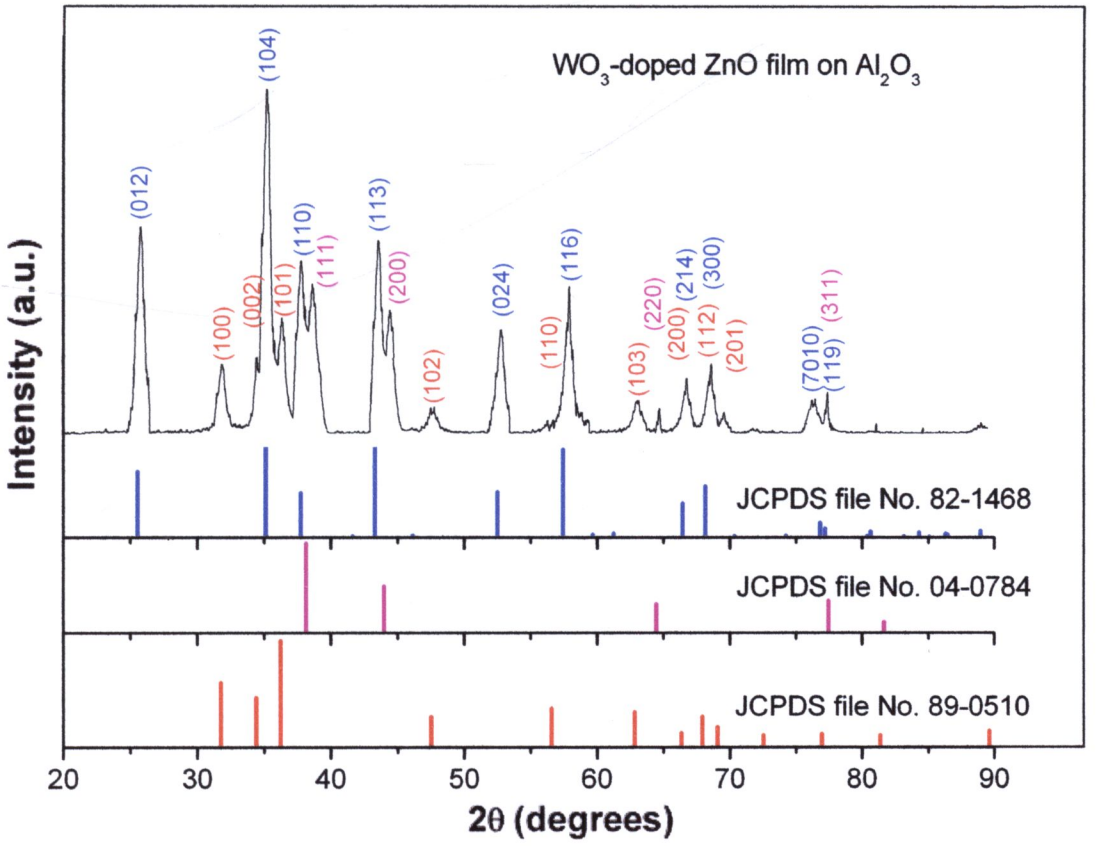

Figure 4.8 XRD pattern of gas sensing film based on flame-made 0.75 mol% WO_3-doped ZnO nanoparticles after anneal and sensing test at 400 °C. JCPDS file No. 89-0510, 04-0784 and 82-1468 refer to ZnO, Au and Al_2O_3, respectively [29-31].

4.3.2 SEM cross-section micrograph and EDS line scan mode

The cross-section and film thickness of gas sensing films based on flame-made pure ZnO and 0.25, 0.50 and 0.75 mol% WO_3-doped ZnO nanoparticles after sensing test at 400°C were observed using SEM analysis with different magnifications

as shown in Figures 4.9, 4.10, 4.11 and 4.12, respectively. It was found that film thickness of pure ZnO and 0.25, 0.50 and 0.75 mol% WO_3-doped ZnO sensors were about 0.984, 1.397, 1.169 and 1.830 μm, respectively. These results could confirm that film thickness of all sensors were in the same range of about 1-2 μm. The Al_2O_3 substrates were also visible in all images.

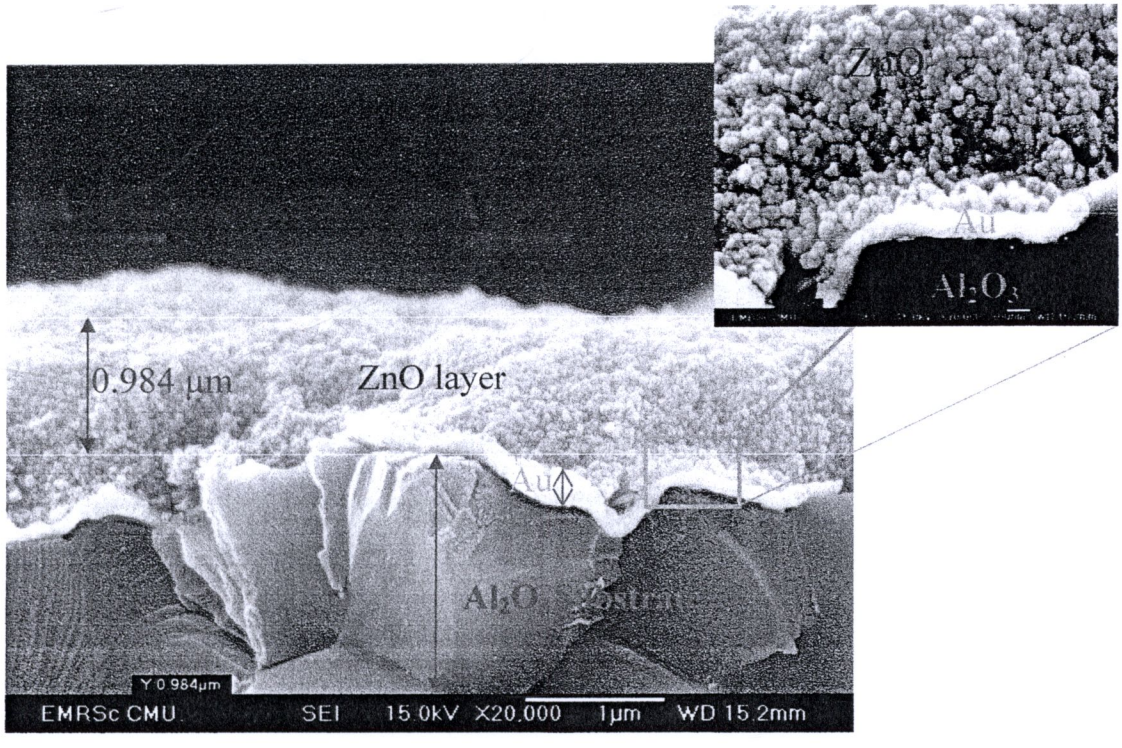

Figure 4.9 Cross-section SEM micrograph of gas sensing film based on flame-made pure ZnO nanoparticles. Inset shows the higher magnification image.

The gold electrode layers of gas sensing films were found in Figures 4.9 and 4.10. The thicknesses of these gold electrodes were in the range of 0.1 μm. Insets in Figure 4.9 and 4.12 show the higher magnification cross-section SEM images. It was found that several nanoparticles were connected with each other but their primary particle sizes were not changed. The particle sizes in the range of 10-25 nm were found in most images.

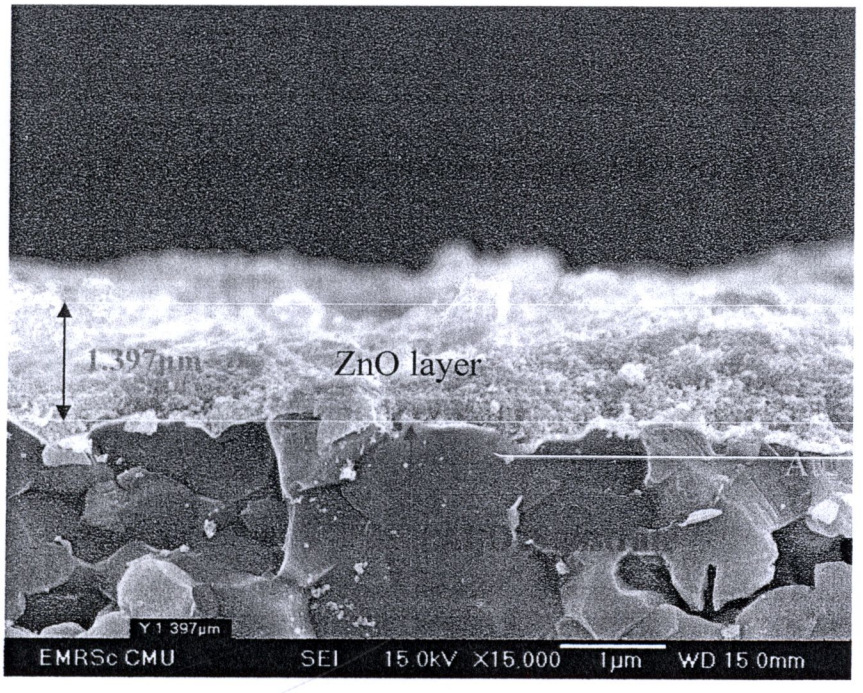

Figure 4.10 Cross-section SEM micrograph of gas sensing film based on flame-made 0.25 mol% WO_3-doped ZnO nanoparticles

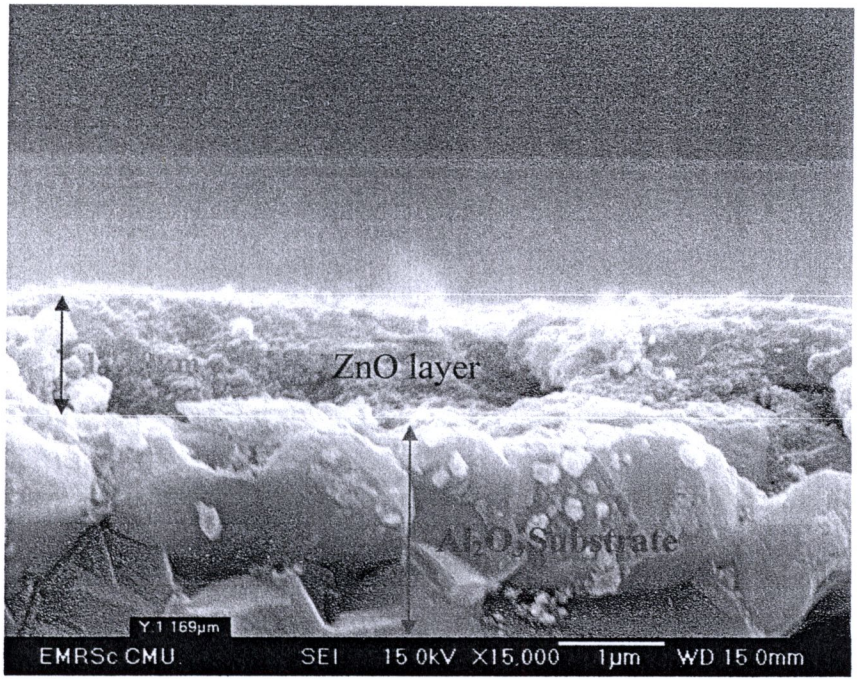

Figure 4.11 Cross-section SEM micrograph of gas sensing film based on flame-made 0.50 mol% WO_3-doped ZnO nanoparticles

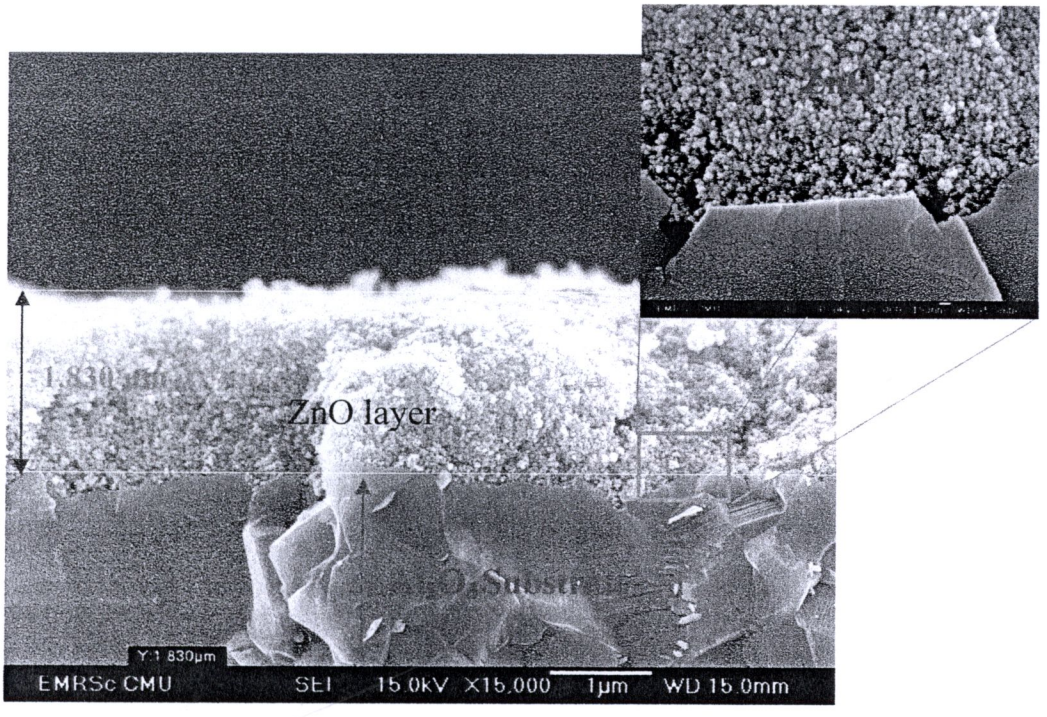

Figure 4.12 Cross-section SEM micrograph of gas sensing film based on flame made 0.75 mol% WO_3-doped ZnO nanoparticles. Inset shows the higher magnification image.

The elemental composition of gas sensing films could be confirmed by Energy Dispersive X-ray Spectrometry (EDS) line scan mode-SEM analysis. The trend in the elemental composition of gas sensing films based on flame-made pure ZnO and 0.25, 0.50 and 0.75 mol% WO_3-doped ZnO nanoparticles were shown in Figures 4.13, 4.14, 4.15 and 4.16, respectively. The results from EDS line scan mode revealed that the elemental composition of gas sensing films corresponded well with the elementals that were indicated in Figures 4.9-4.12. The line scans showed the elemental histograms corresponding to a rich in alumina caused by the Al_2O_3 substrate, poor gold (Au) caused by both an Au electrode and Au sputtering prior to the analysis, zinc (Zn), poor tungsten (W) and oxygen (O).

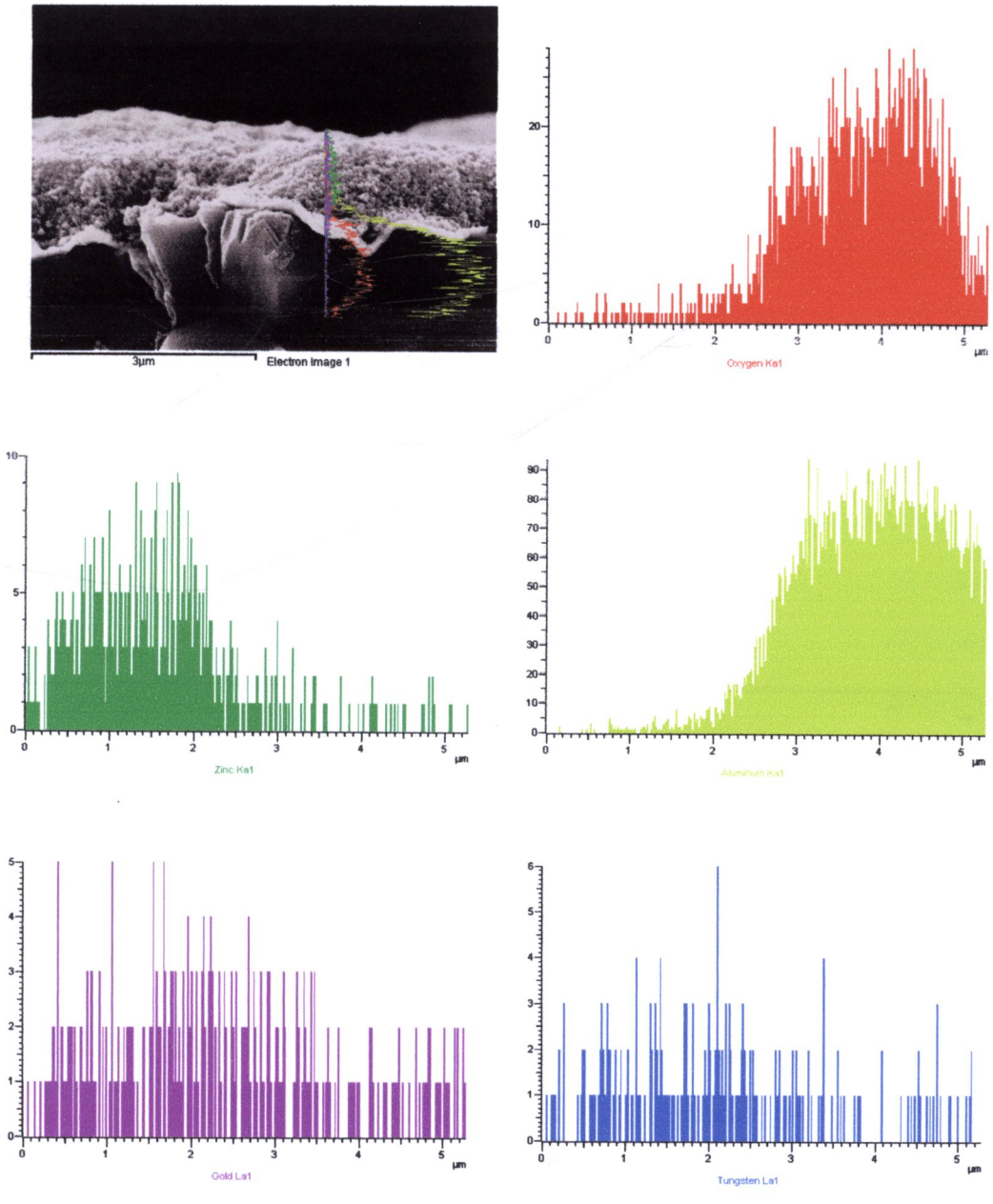

Figure 4.13 The EDS line scan mode-SEM analysis of sensor based on flame-made pure ZnO nanoarticles. The histograms showed the elemental compositions of samples. The lines scans correspond to O, Zn, Al, Au and W elements.

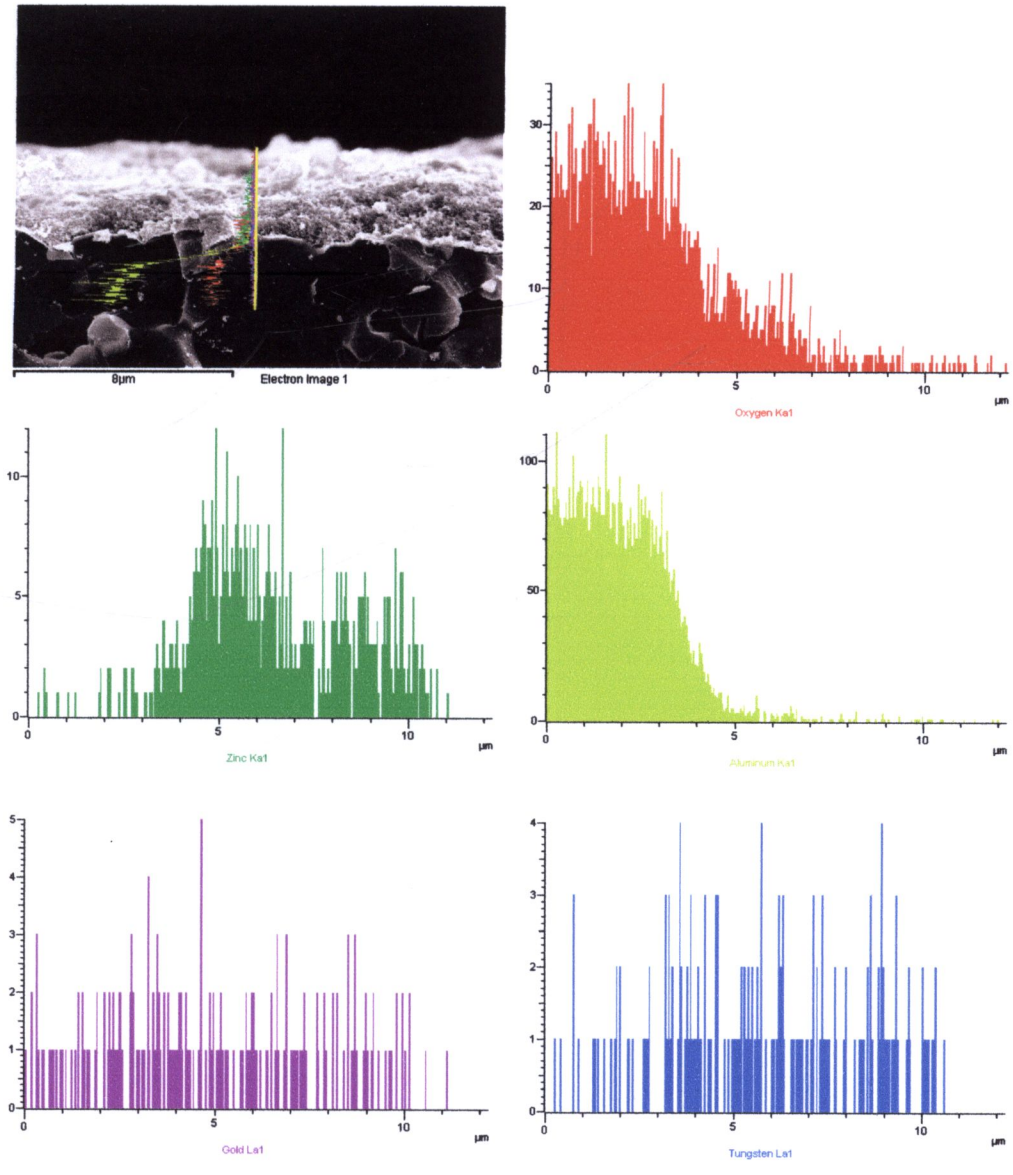

Figure 4.14 The EDS line scan mode-SEM analysis of sensor based on flame-made 0.25 mol% WO_3-doped ZnO nanoarticles. The histograms showed the elemental compositions of samples. The lines scans correspond to O, Zn, Al, Au and W elements.

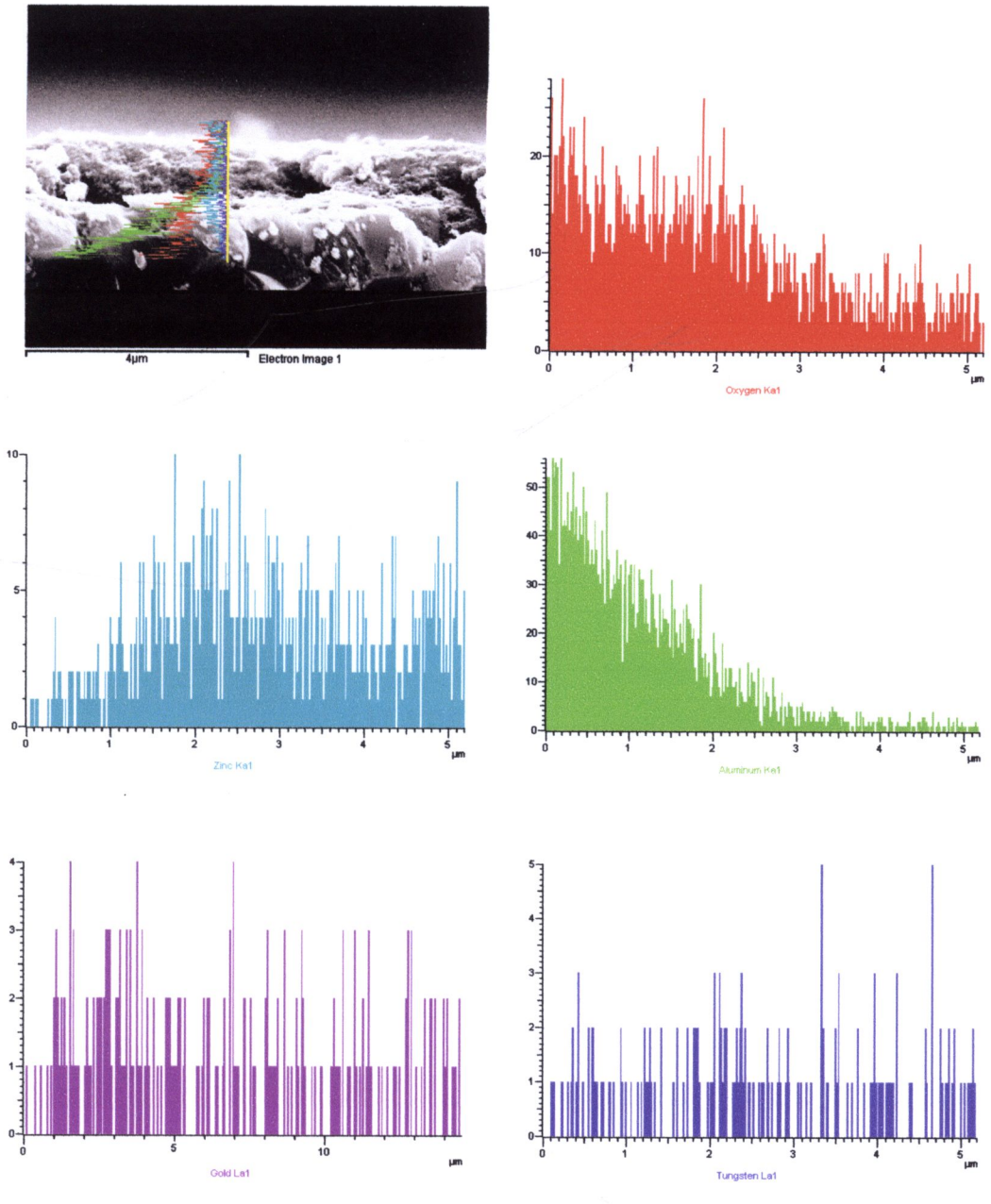

Figure 4.15 The EDS line scan mode-SEM analysis of sensor based on flame-made 0.50 mol% WO_3-doped ZnO nanoarticles. The histograms showed the elemental compositions of samples. The lines scans correspond to O, Zn, Al, Au and W elements.

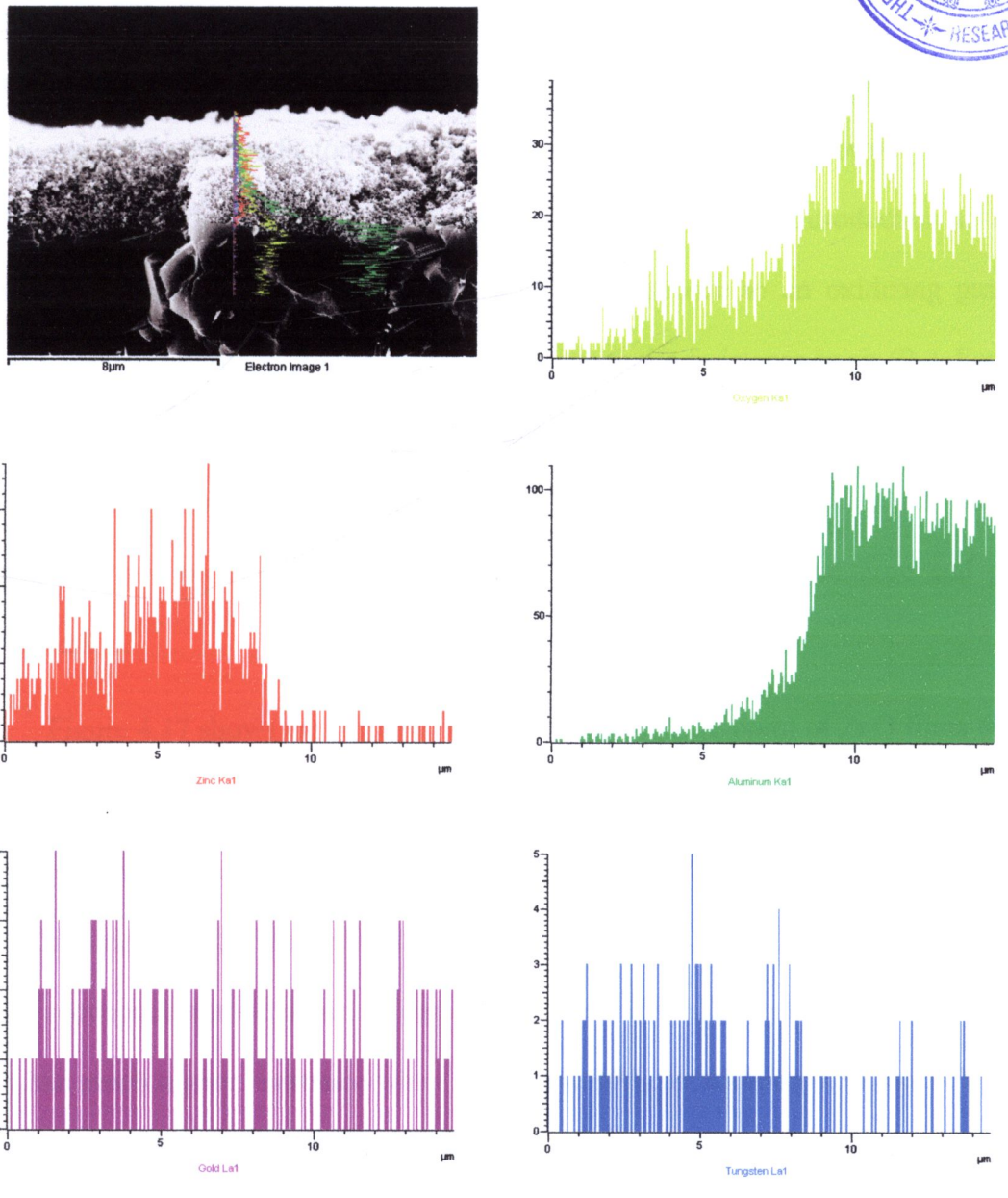

Figure 4.16 The EDS line scan mode-SEM analysis of sensor based on flame-made 0.75 mol% WO_3-doped ZnO nanoarticles. The histograms showed the elemental compositions of samples. The lines scans correspond to O, Zn, Al, Au and W elements.

4.3.3 Gas sensing characteristic

The gas sensing properties are characterized in terms of dynamic change of resistance and gas-sensing sensitivity. The gas sensing sensitivity of n-type semiconductor based conductometric gas sensor to a reducing gas is normally defined as the ratio, $\Delta R/Rg$, of the resistance change (ΔR) due to gas introduction to the resistance when the gas is present (Rg) while the response to an oxidizing gas is defined as the ratio, $\Delta R/R_0$, of the resistance change to the resistance in air (R_0). For p-type semiconductor gas sensor, the definitions are reversed. The gas-sensing sensitivity was calculated from dynamic variation of the conductance due to gas pulses introduction and plotted versus various parameters including temperature and gas concentration.

Figure 4.17 shows the dynamic response to NO_2 (1-50 ppm) of ZnO films with difference WO_3 contents at operating temperature of 400°C. It can be seen that the resistant of all ZnO sensors increased upon the exposure to NO_2 which is an oxidizing gas, indicating that both the undoped ZnO and WO_3-doped ZnO films show the typical n-type semiconductor behavior. Comparing to pure ZnO film, all WO_3-doped ZnO films had much higher resistance when exposed to NO_2. In addition 0.50 mol% WO_3-doped ZnO film showed the highest response to NO_2. These results could be assumed that the gas sensing properties of ZnO nanoparticle films could be greatly improved by doping with an appropriate amount of WO_3.

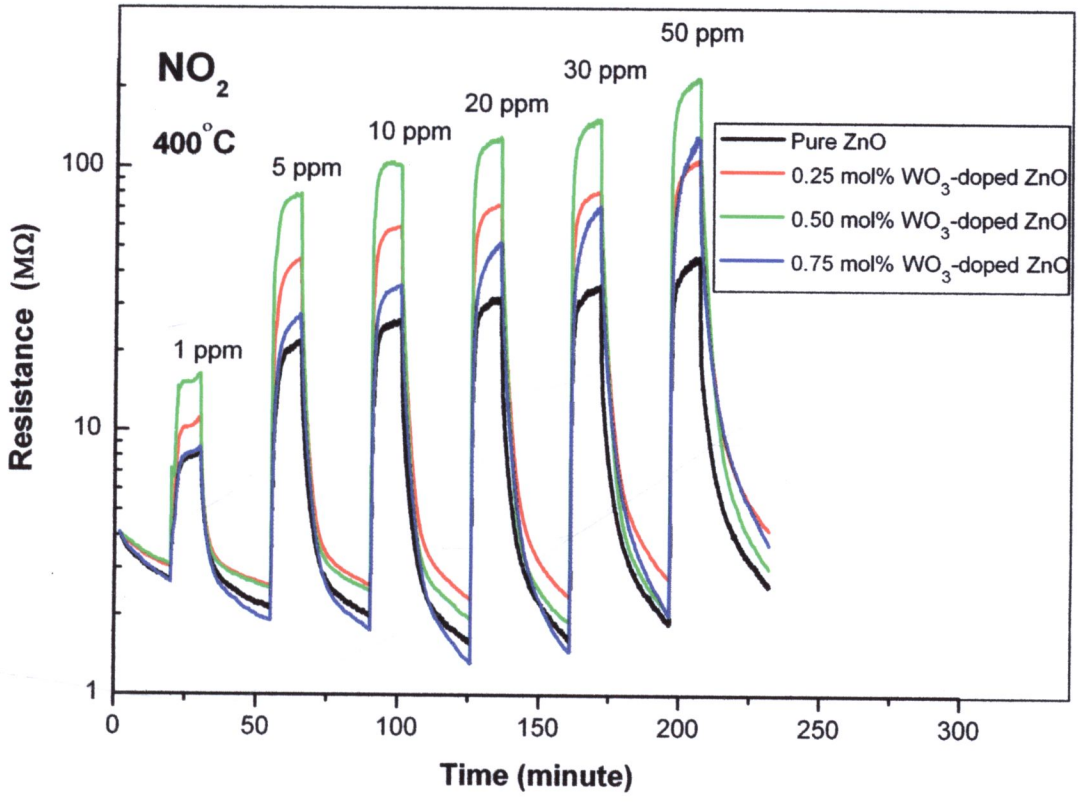

Figure 4.17 NO_2 response of WO_3-doped ZnO with different WO_3 concentrations vs. time towards 1, 5, 10, 20, 30 and 50 ppm square pulses at 400°C

The calculated sensitivities towards NO_2 at 50 ppm concentration versus operating temperature of pure ZnO and WO_3-doped ZnO films are shown in Figure 4.18. It can be noticed that the sensitivities of 0.50 and 0.75 mol% WO_3 doped ZnO films towards NO_2 were improved comparing to undoped ZnO at all operating temperatures. The sensitivity of 0.25 mol% WO_3 doped ZnO film towards NO_2 was comparable to undoped ZnO at low operating temperature but it was higher than that of undoped ZnO at operating temperature of 400°C. In addition, the sensitivity of all WO_3-doped ZnO films tended to increase with operating temperature. On the contrary, the sensitivity of pure ZnO tended to decrease with operating temperature. Moreover,

the 0.50 mol% WO_3-doped ZnO film had higher sensitivity towards NO_2 than the pure ZnO film by the order of five at the operating temperature of 400°C.

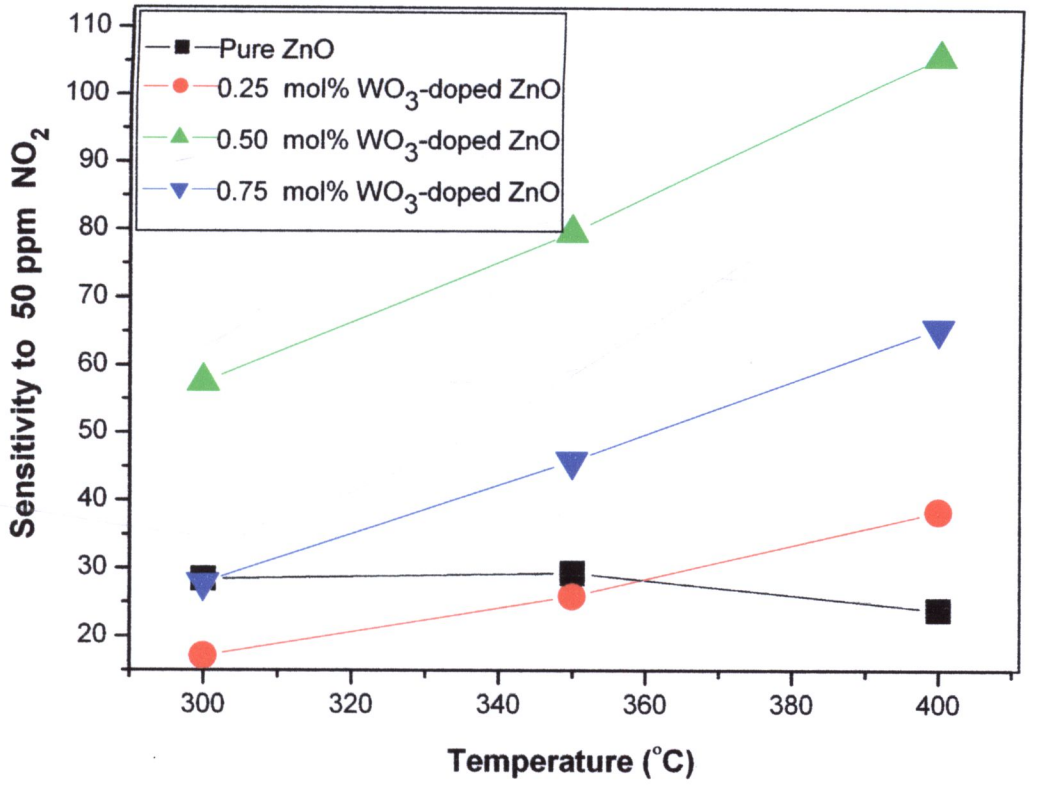

Figure 4.18 NO_2 sensitivity of WO_3-doped ZnO with different WO_3 concentrations vs. operating temperature at 50 ppm concentration

The dynamic response to C_2H_5OH (100-1,000 ppm) of ZnO films with difference WO_3 contents at operating temperature of 400°C is shown in Figure 4.19. It can be seen that the resistant of all ZnO sensors decreased upon the exposure to C_2H_5OH which is a reducing gas, indicating that both the undoped ZnO and WO_3 doped ZnO films still behave as n-type semiconductor. The resistances of all WO_3 doped ZnO films were much lower than undoped ZnO when exposed to C_2H_5OH at any concentrations. Moreover for the doped samples, the 0.50 mol% WO_3-doped ZnO film still showed the highest response to this gas.

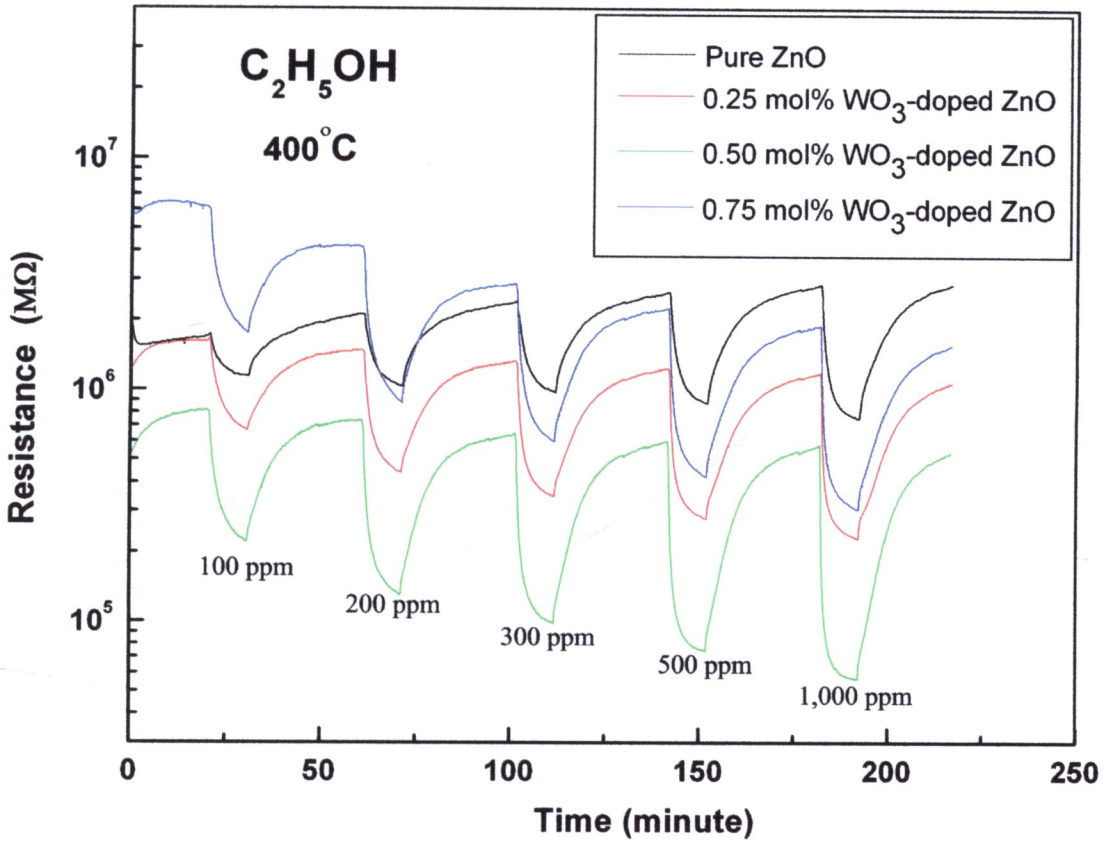

Figure 4.19 C_2H_5OH response of WO_3-doped ZnO with different WO_3 concentrations vs. time towards 100, 200, 300, 500 and 1,000 ppm square pulses at 400°C

The calculated sensitivities towards C_2H_5OH at 1,000 ppm concentration versus operating temperature of pure ZnO and WO_3-doped ZnO films are shown in Figure 4.20. It can be noticed that the sensitivities of all WO_3 doped ZnO films towards C_2H_5OH were improved comparing to undoped ZnO. The sensitivity of 0.25 and 0.75 mol% WO_3 doped ZnO film towards C_2H_5OH were comparable to undoped ZnO at operating temperature of 300°C but they were obviously higher than that of undoped ZnO at operating temperature of 350 and 400 °C. The sensitivity of 0.50 mol% WO_3 doped ZnO films showed the highest sensitivity at all operating temperature. In addition, the sensitivity of both undoped ZnO and WO_3-doped ZnO

films tended to increase with operating temperature. Moreover, the 0.50 mol% WO_3-doped ZnO film had higher sensitivity towards C_2H_5OH than the pure ZnO film by the order of three at the operating temperature of 400°C.

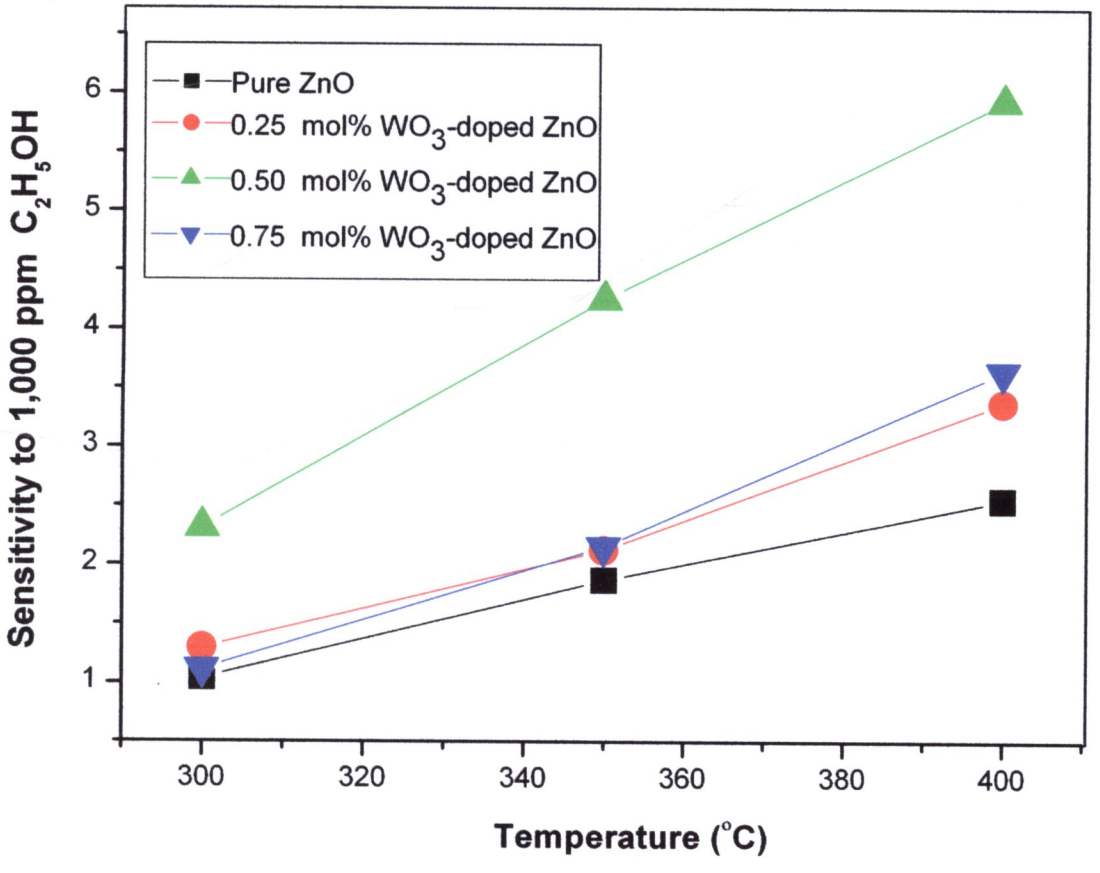

Figure 4.20 C_2H_5OH sensitivity of WO_3-doped ZnO with different WO_3 concentrations vs. operating temperature at 1,000 ppm concentration

The dynamic response to CO (50-1,000 ppm) of ZnO films with different WO_3 contents at operating temperature of 400°C are shown in Figure 4.21. It can be seen that the resistant of all ZnO sensors decreased upon the exposure to CO which is a reducing gas, indicating that both the undoped ZnO and WO_3 doped ZnO films still behave as n-type semiconductor. The resistances of all WO_3 doped ZnO films were comparable to pure ZnO film when exposed to CO at any concentrations. Therefore, the WO_3 doping did not much effect to the response of ZnO sensors towards CO.

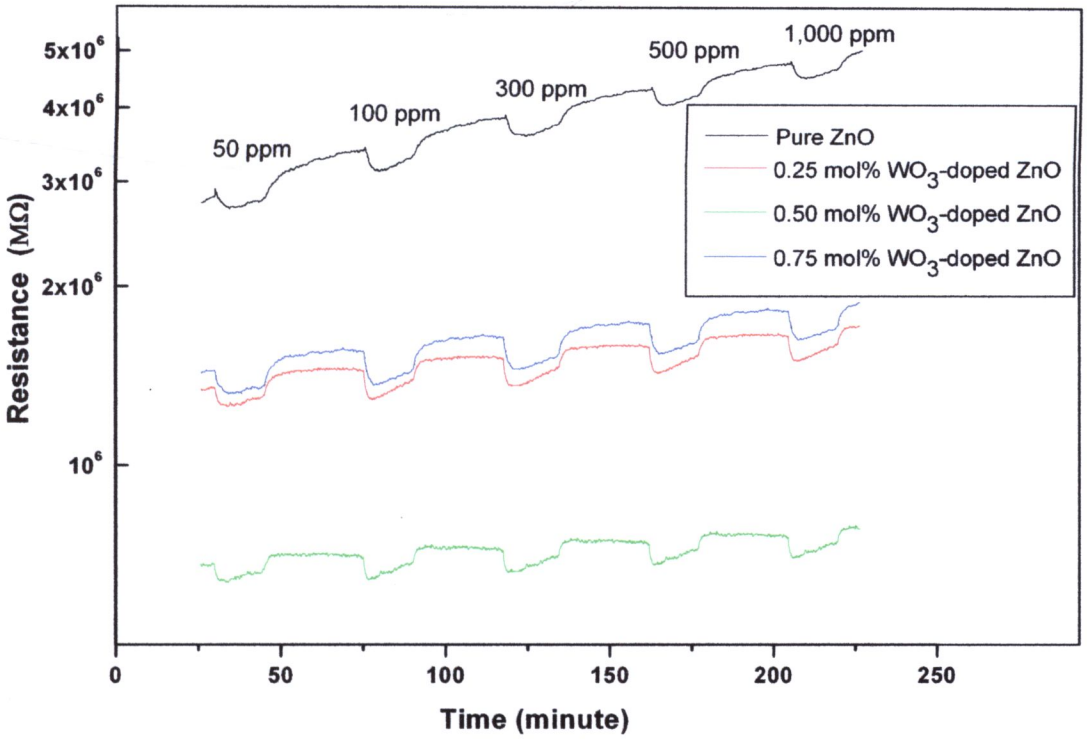

Figure 4.21 CO response of WO_3-doped ZnO with different WO_3 concentrations vs. time towards 50, 100, 300, 500 and 1,000 ppm square pulses at 400°C

The calculated sensitivities towards CO at 1,000 ppm concentration versus operating temperature of pure ZnO and WO_3-doped ZnO films are shown in Figure 4.22. It can be seen that the WO_3 doping resulted in a little sensitivity improvement

behaviors at the operating temperature of 400 °C. However, the sensitivity of n-type ZnO film was too small and almost negligible compared to the NO_2 and C_2H_5OH case. In addition, the CO sensitivity of all films tended to increase with the operating temperature.

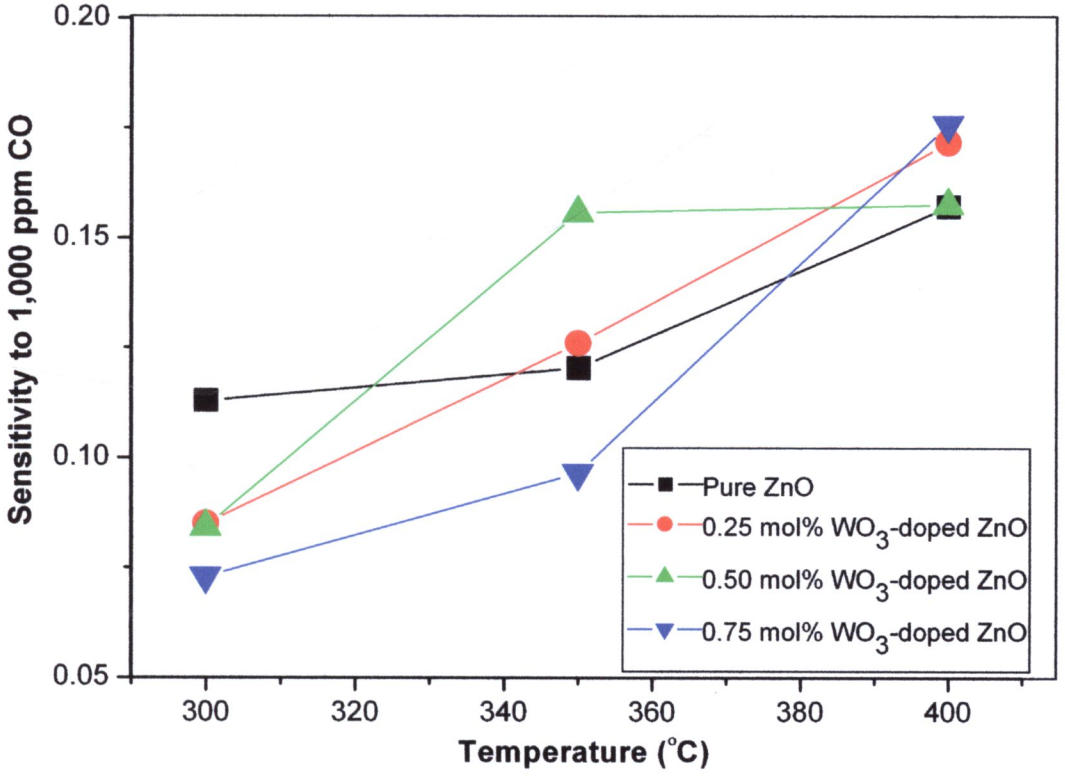

Figure 4.22 CO sensitivity of WO_3-doped ZnO with different WO_3 concentrations vs. operating temperature at 1,000 ppm concentration

Figure 4.23 shows the dynamic response to H_2 (500-10,000 ppm) of ZnO films with difference WO_3 contents at operating temperature of 400°C. It can be seen that the resistant of all ZnO sensors increased upon the exposure to H_2 which is an oxidizing gas, indicating that both the undoped ZnO and WO_3-doped ZnO films still behave as n-type semiconductor behavior. Comparing to pure ZnO film, all WO_3-doped ZnO

films had higher resistance when exposed to H_2. However, the increasing of resistance of n-type ZnO films was too small compared to the NO_2 case.

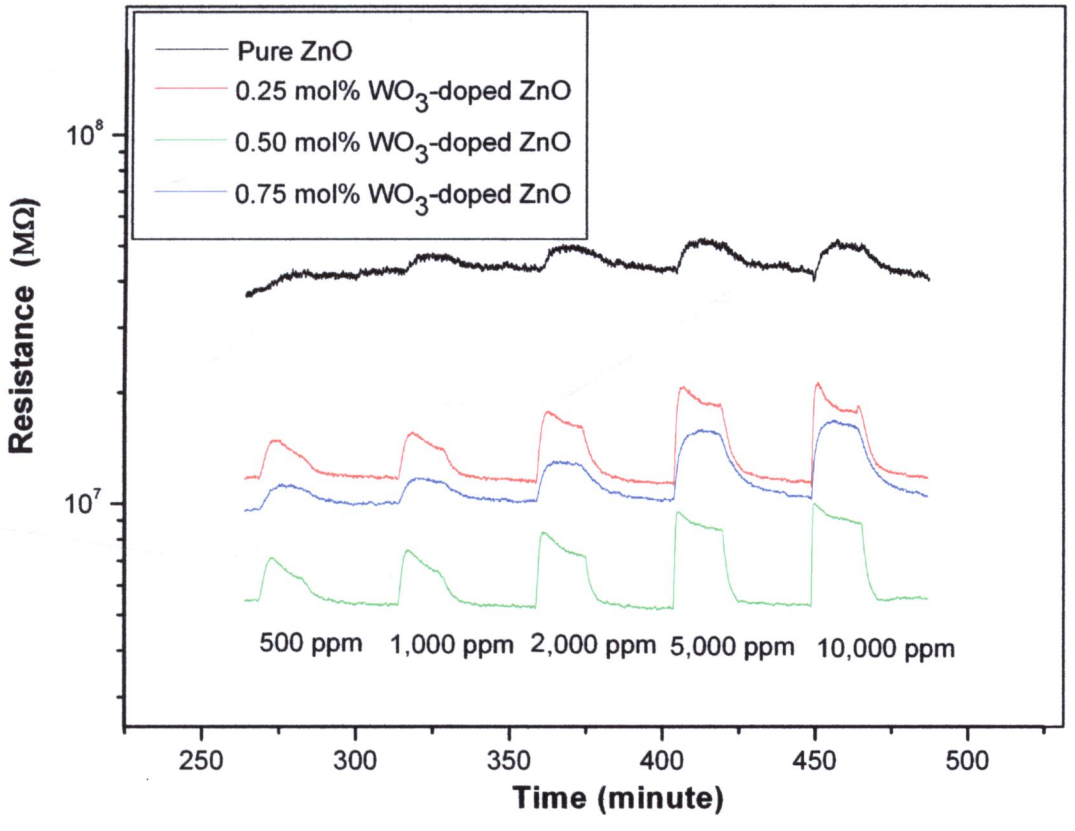

Figure 4.23 H_2 response of WO_3-doped ZnO with different WO_3 concentrations vs. time towards 500, 1,000, 2,000, 5,000 and 1,000 ppm square pulses at 400°C

Figure 4.24 shows the calculated sensitivities towards H_2 at 2,000 ppm concentration versus operating temperature of pure ZnO and WO_3-doped ZnO films. It can be noticed that the WO_3 doping seemed not much to influence in the sensitivity towards H_2 and the sensitivity was very low and independent of operating temperature.

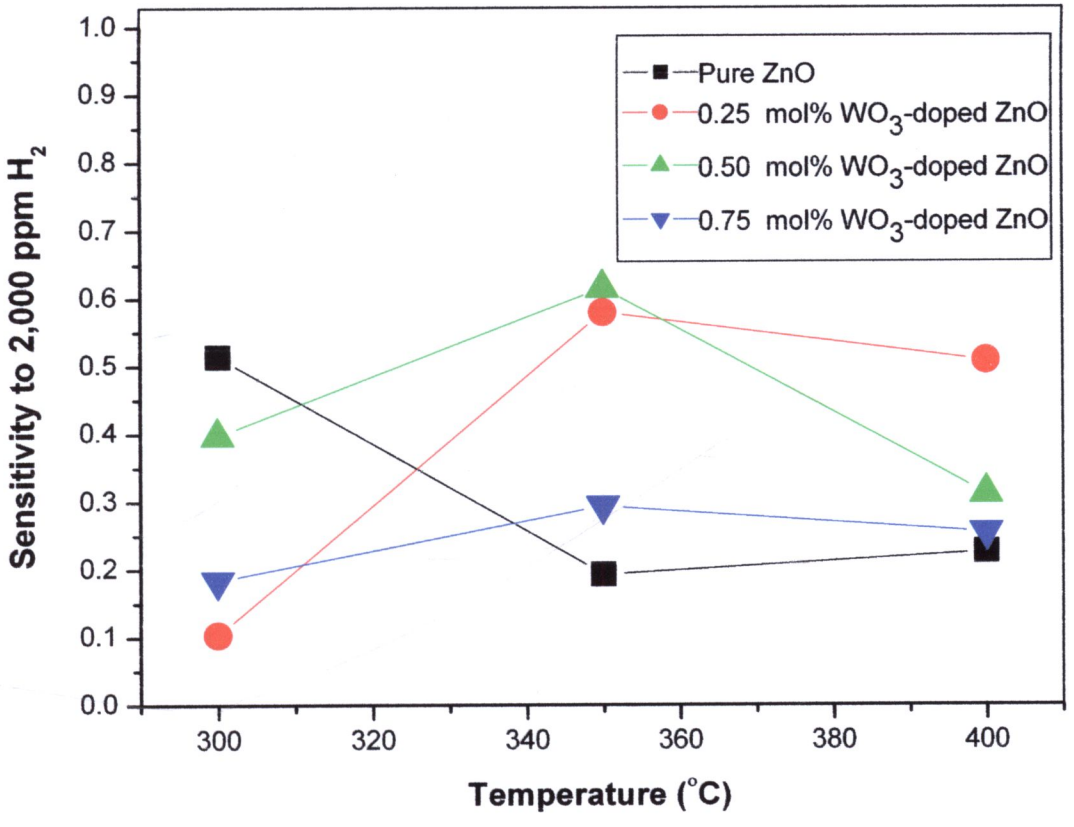

Figure 4.24 H_2 sensitivity of WO_3-doped ZnO with different WO_3 concentrations vs. operating temperature at 2,000 ppm concentration

The comparison of sensitivity of WO_3-doped ZnO with different WO_3 concentrations towards 50 ppm of NO_2, 1,000 ppm of C_2H_5OH, 1,000 ppm of CO and 1,000 ppm of H_2 at 400°C is shown in Figure 4.25. It can be noticed that the sensitivities of all WO_3-doped ZnO films toward NO_2 and C_2H_5OH were clearly improved comparing to undoped ZnO. The sensitivities of all ZnO films towards NO_2 were greatly higher than that towards C_2H_5OH, CO and H_2. Moreover, the sensitivities of ZnO films towards CO and H_2 were too small and almost negligible compared to the NO_2 case. Namely, these gas sensing WO_3-doped ZnO films had a high selectivity towards NO_2.

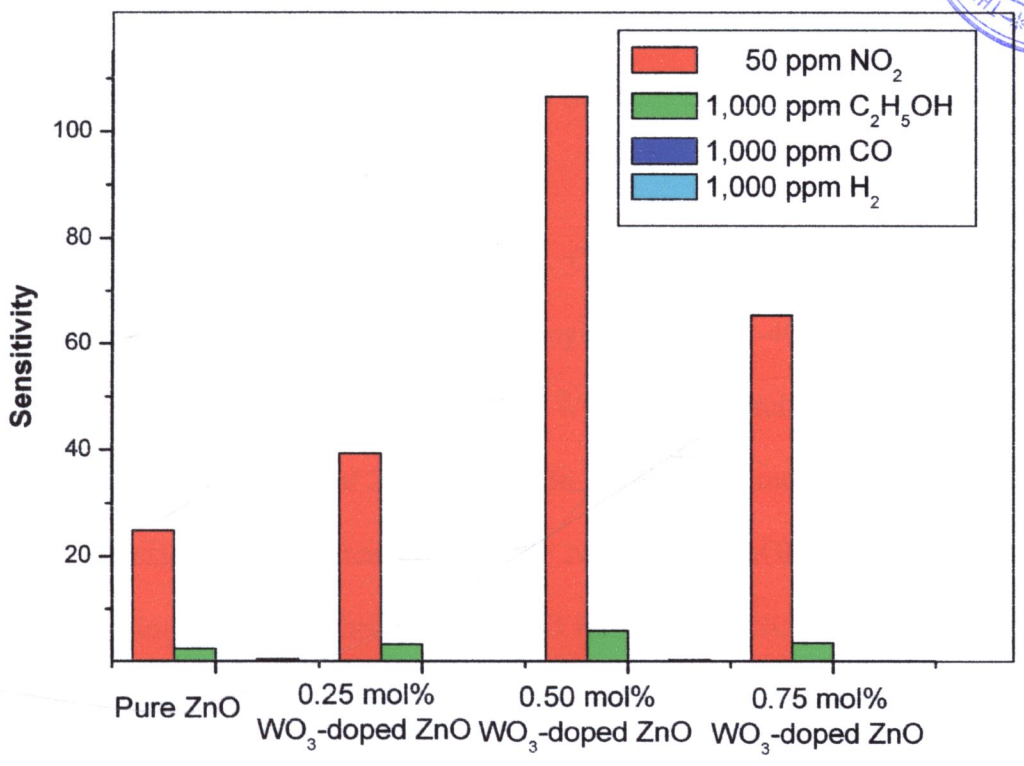

Figure 4.25 The comparison of sensitivity of WO_3-doped ZnO with different WO_3 concentrations towards 50 ppm of NO_2, 1,000 ppm of C_2H_5OH, 1,000 ppm of CO and 1,000 ppm of H_2 at 400°C

4.4 Conclusions

The sensing films were produced by mixing pure, 0.25, 0.50 and 0.75 mol% WO_3-doped ZnO nanoparticles into an organic paste and the resulting paste was spin-coated on Al_2O_3 substrates interdigitated with Au electrodes. Before gas sensor testing, they were annealed in air at 400 °C for 2h for binder removal. The crystalline phase, morphology and composition of gas sensing films based on flame-made undoped ZnO and WO_3-doped were observed by XRD, SEM and EDS. The XRD patterns showed that the nanoparticle films had the hexagonal phase of ZnO with the JCPDS file No.89-0510. Al_2O_3 and Au from substrate were also visible in these patterns. The

cross-section SEM micrographs revealed that film thickness of all sensors were in the same range about 1-2 μm. The compositions of SEM micrographs including Zn, O, Au and Al were verified by EDS method.

The sensors were tested towards NO_2, C_2H_5OH, CO and H_2 at different gas concentrations and operating temperatures ranging from 300-400°C in dry air. The results showed that the appropriate amount of WO_3 loading could greatly enhance the NO_2 and C_2H_5OH sensitivity of ZnO sensors. In addition, 0.5 mol% WO_3-doped ZnO nanoparticles exhibited maximum response to NO_2 and C_2H_5OH at all temperatures and concentrations. The sensitivities of all ZnO films toward NO_2 were greatly higher than that towards C_2H_5OH, CO and H_2. Nevertheless, hydrogen sensitivity was relatively less improved by WO_3 doping while sensitivity toward CO was almost insensitive to WO_3 content, therefore WO_3-doped ZnO sensor had a high selectivity towards NO_2.

REFERENCES

1. Xiangfeng C., Dongli J., Djurišc A.B., Leung Y.H. Gas-sensing properties of thick film based on ZnO nano-tetrapods, *Chem. Phys. Lett.*, 2005, **401**, 426-429.
2. Hongsith N., Viriyaworasakul C., Mangkorntong P., Mangkorntong N., Choopun S. Ethanol sensor based on ZnO and Au-doped ZnO nanowires, *Ceram. Int.*, 2008, **34**, 823-826.
3. Kim S.J., Choa P.S., Leea J.H., Kangb C.Y., Kimb J.S., Yoon S.J. Preparation of multi-compositional gas sensing films by combinatorial solution deposition, *Ceram. Int.*, 2008, **34**, 827–831.
4. Müller R., Mädler L., Pratsinis S.E., Nanoparticle synthesis at high production rates by flame spray pyrolysis, *Chem. Eng. Sci.*, 2003, **58**, 1969-1976.
5. Tani T., Mädler L., Pratsinis S.E. Homogeneous ZnO nanoparticles by flame spray pyrolysis, *J. Nanopart. Res.*, 2002, **4**, 337-343.
6. Height M.J., Pratsinis S.E., Mekasuwandumrong O. Ag-ZnO catalysts for UV-photodegradation of methylene blue, *Appl. Catal. B-Environ.*, 2006, **63**, 305- 312.
7. Height M.J., Mädler L., Krumeich F., Pratsinis S.E. Nanorods of ZnO Made by Flame Spray Pyrolysis, *Chem. Mater.*, 2006, **18**, 572-578.
8. Eggins, B.R. *Chemical Sensors and Biosensors.* John Wiley & Sons, West Sussex, 2002.
9. Min, Y. *Properties and Sensor Performance of Zinc Oxide Thin Films*. Ph. D. Thesis, Massachusetts Institute of Technology, 2003.
10. Janata, J. *Principles of Chemical Sensors.* Plenum Press, New York 1989.

11. Yamazoe N., Fuchigami J., Kishikawa M., Seiyama T. Interactions of tin oxide surface with O_2, H_2O, and H_2, *Surf. Sci.*, 1979, **86**, 335-344.

12. Göpel W., Schierbaum K.D. SnO_2 sensors: current status and future prospect, *Senser Actuat. B-Chem.*, 1995, **26-27**, 1-12.

13. Shimizu Y., Egashira M. Basic Aspects and challenges of semiconductor gas sensor, *MRS Bull.*, 1999, **6**, 18-24.

14. Teleki, A., Pratsinis, S. E., Kalyanasundaram, K., Gouma, P.I. Sensing of organic vapors by flame-made TiO_2 nanoparticles. *Senser. Actuat. B-Chem.*, 2006, **119**, 683-690.

15. Nunes P., Fortunato E., Lopes A., Martins R. Influence of the deposition conditions on the gas sensitivity of zinc oxide thin films deposited by spray pyrolysis, *Int. J. Inorg. Mater.*, 2001, **3**, 1129-1131.

16. Cheng X.L., Zhao H., Huo L.H., Gao S., Zhao J.G. ZnO nanoparticulate thin film: preparation, characterization and gas-sensing property, *Sensor Actuat. B-Chem*, 2001, **102**, 248-252.

17. Chang J.F., Kuo H.H., Leu I.C., Hon M.H. The effects of thickness and operation temperature on ZnO:Al thin film CO gas sensor, *Sensor Actuat. B-Chem*, 2002, **84**, 258-264.

18. Mitra P., Chatterjee A.P., Maiti H.S. ZnO thin film sensor, *Mater. Lett.*, 1998, **35**, 33-38.

19. Sahay, P. P., Tewari, S., Jha, S., Shamsuddin, M. Sprayed ZnO thin films for ethanol sensor, *J. Mater. Sci.*, 2005, **40**, 4791-4793.

20. Rao G.S.T., Rao D.T., Gas sensitivity of ZnO based thick film sensor to NH_3 at room temperature, *Sensor Actuat. B-Chem*, 1999, **55**, 166-169.

21. Paraguay F.D., Yoshida M.M., Morales J.J., Solis J., Estrada W.L. Influence of Al, In, Cu, Fe and Sn dopants on the response of thin film ZnO gas sensor to ethanol vapour, *Thin Solid Flims*, 2000, **373**, 137-140.

22. Wang X., Zhang J., Zhu Z., Zhu J. Effect of Pd^{2+} doping on ZnO nanotetrapods ammonia sensor, *Colloid. Surface A*, 2005, **276**, 59-64.

23. Chung Y.K., Kim M.H., Um W.S., Lee H.S., Song J.K., Choi S.C., Yi K.M., Lee M.J., Chung K.W. Gas sensing properties of WO_3 thick film for NO_2 gas dependent on process condition, *Sensor Actuat. B-Chem*, 1999, **60**, 49-56.

24. Kim S.J., Choa P.S., Leea J.H., Kangb C.Y., Kimb J.S., Yoon S.J. Preparation of multi-compositional gas sensing films by combinatorial solution deposition, *Ceram. Int.*, 2008, **34**, 827–831.

25. Müller R., Mädler L., Pratsinis S.E. Nanoparticle synthesis at high production rates by flame spray pyrolysis, *Chem. Eng. Sci.*, 2003, **58**, 1969-1976.

26. Tani T., Mädler L., Pratsinis S.E. Homogeneous ZnO nanoparticles by flame spray pyrolysis, *J. Nanopart. Res.*, 2002, **4**, 337-343.

27. Height M.J., Pratsinis S.E. and Mekasuwandumrong O. Ag-ZnO catalysts for UV-photodegradation of methylene blue, *Appl. Catal. B-Environ.*, 2006, **63**, 305- 312.

28. Height M.J., Mädler L., Krumeich F., Pratsinis S.E. Nanorods of ZnO Made by Flame Spray Pyrolysis, *Chem. Mater.*, 2006, **18**, 572-578.

29. Sawada H., Wang R., Sleight A.W. An Electron Density Residual Study of Zinc Oxide, *J. Solid State Chem.*, 1996, **122**, 148-150.

30. Sawada, H. Residual electron density study of α-aluminum oxide through refinement of experimental atomic scattering factors, *Mater. Res. Bull.*, 1994, **29**, 127-133.

31. Wong-Ng W., McMurdie H.F., Hubbardl C.R., Mighell A.D. JCPDS-ICDD Research Associateship(Cooperative Program with NBS/NIST), J. *Res. Natl. Inst. Stan.*, 2001, **106**, 1013-1028.